AN INTEGRATED MEMS FERROFLUID PUMP USING INSULATED METAL SUBSTRATE

Leidong Mao and Hur Koser
Yale University
Department of Electrical Engineering
15 Prospect Street
New Haven, CT 06520, USA
Leidong.Mao@yale.edu
Hur.Koser@yale.edu

***Abstract* – A novel ferrofluid micropump utilizing traveling magnetic fields is designed based on previous numerical analysis. A cost-effective fabrication process combining insulated metal substrate etching and soft lithography is used to realize the prototype ferrofluid micropump. Preliminary results show good agreement of pumping characteristics between theory and experiment.**

I. INTRODUCTION

Ferrofluids are stable colloidal suspensions of nanosize ferromagnetic particles in either aqueous or oil-based media. A magnetic field gradient, combined with liquid viscous forces, allows continuous actuation and precise positioning of a ferrofluid segment in a flow channel [1]. Ferrofluids have found their way into a variety of applications, such as sealing, damping and blood separation [2]. Recently, manipulation of ferrofluids in a magnetic micropump and a magnetic fluid linear pump were demonstrated, but actuation was achieved using external, macro-scale magnetic windings or permanent magnets, and the actuation speed was limited [3, 4]. In dilute, functionalized forms, ferrofluids have also been used as drug delivery and MRI contrast agents [5]. Ferrofluids offer attractive alternatives to moving mechanical components in miniaturized cooling, pumping and integrated micro-total-analysis-systems for chip-scale chemistry and biology. Water-based ferrofluids can be made bio-compatible, rendering them useful in novel cell manipulation and sorting schemes. Here, we present a new, integrated ferrofluid micropump design and a prototype device that achieves high flow rates. The micropump consists of two parts: the microfluidic channel and the excitation electrodes fabricated on a thermal clad insulated metal substrate (IMS) printed circuit board (PCB). This device requires no external moving mechanical parts for actuation, and is suitable for fully-integrated microfluidic circuits.

II. THEORY

Ferrofluid pumping in spatially uniform, sinusoidally time-varying magnetic fields has been studied extensively in the past [6]. Our design is based on spatially traveling sinusoidal magnetic fields, which offer the advantage of utilizing both magnetic force and magnetic torque pumping to achieve high flow rates [7, 8]. Our approach involves solving the magnetization constitutive equation with coupled linear and angular momentum conservation equations to model the behavior of ferrofluids in microchannels in the presence of spatially traveling magnetic fields. An iterative, second-order central-differencing scheme has been employed to calculate the magnetic field, particle spin velocity and overall flow velocity inside the ferrofluid. The schematic diagram of the device configuration is shown in Fig. 1.

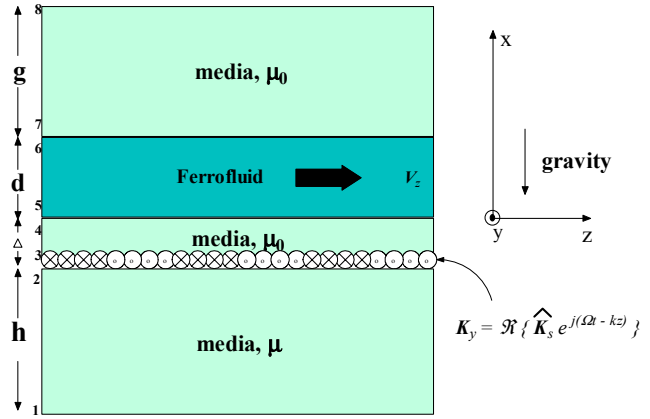

Fig. 1. A planar ferrofluid layer inside a microfluidic channel is magnetically stressed by a traveling wave current sheet. The top layer is taken thick enough to represent an infinite boundary.

In this configuration, flow velocity for a given ferrofluid depends partly on the spatial period of the traveling wave and the channel dimension; the frequency of the input excitation precisely controls the flow speed. Flow can be reversed by changing the traveling magnetic field direction. As shown in Fig. 2, maximum flow velocity is achieved when the product of the excitation wavenumber and height of the ferrofluid channel approaches unity, and the excitation frequency is close to the reciprocal of the relaxation time constant of magnetic particles [7-9].

III. FABRICATION

Fig. 3 depicts the process flow and an initial prototype of the ferrofluid micropump designed based on previous numerical analysis. The fabrication process is comprised of two parts: copper electrodes fabricated on an IMS – steps (a) through (f) – and ferrofluid microfluidic channels realized by soft lithography – steps (g) through (k) [10]. In this section, fabrication steps shown in Fig. 3 are discussed in detail.

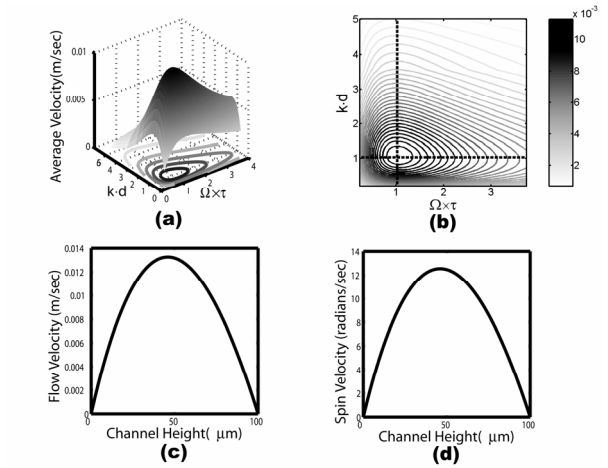

Fig. 2. 3-D (a) and contour (b) plot of average flow velocity of ferrofluid versus the product of wave number and the height of the channel ($k \times d$) for various applied magnetic field frequencies. The Brownian relaxation time constant for the nanoparticles (τ), as well as the geometry determine the pumping peak. The flow velocity (c) and particle spin velocity (d) profiles across the height of the microchannel are also shown. Here, K_s = 10000 A/m, height of channel d = 100 μm, traveling wave period $\lambda = 2\pi/k$ = 1.26 mm, χ_0 = 1.17, τ = 3.75 μs, η = 0.0045 Kg/m.s, ζ = 0.00039 Kg/m.s, η' = 10^{-9} Kg/m.s (refer to [7] for symbol meanings). Relevant material properties correspond to the EMG 700 series ferrofluid (from FERROTEC) used in actual experiments. The excitation frequency is 42 kHz, chosen to correspond to maximum pumping given τ.

(a) *Substrates:* Two kinds of substrates are used in this process for the purposes of comparison. One of them is the common PC board constructed of 1/16" glass epoxy with a 35 μm thick copper layer on the top side; the other is a commercial thermal clad IMS, chosen for its superior heat conduction capability, mechanical robustness and low cost. The IMS printed circuit board used in this study (Bergquist T-clad) is comprised of three layers: 35 μm thick copper for the circuit layer, 75 μm of dielectric layer with minimum thermal resistance, and a 1.6 mm thick aluminum base layer for easy heat removal.

(b) *SU-8 photoresist and Omnicoat spin-on:* Commonly used photoresists, such as Shipley 1813, often peel off during the high temperature wet etching of copper. Hence, SU-8 50 negative photoresist from MICROCHEM is used in this process as a durable wet etching mask to pattern the copper electrodes. A thin layer of Omnicoat (about 17 nm) between the copper and the photoresist improves adhesion and facilitates the easy removal of the SU-8 after patterning.

(c) *SU-8 photoresist patterning:* After the soft bake step, SU-8 photoresist is exposed under an EVG 620 mask aligner, post-baked and developed to open the etching windows over the copper layer. Before wet etching, the omnicoat layer in the etching windows is removed by the MICROPOSIT MF 319 developer.

(d) *Copper layer wet etching:* Ferric chloride solution at 60°C is used to etch copper. The typical copper electrode dimensions are 240 μm in width and 2.5 cm in length, with 80 μm spacing between two electrodes. In order to get a uniform etch rate for all electrodes, constant agitation during etching is required.

(e) *SU-8 and Omnicoat removal:* The substrate is immersed into Remover PG solution from MICROCHEM at 80°C for 30 seconds. The resulting copper surface is clean and ready for wire-bonding.

(f) *Wire bonding and PDMS spin-on:* The copper electrodes are connected by wire bonds to form a two-phase traveling magnetic field when excited by sinusoidal currents. In order to accommodate high electric currents, multiple aluminum wire bonds are performed on each connection pad using a WESTBOND 7400E bonder. Afterwards, the wire bonds are encapsulated by epoxy for mechanical robustness. A 50 μm thick layer of the elastomer polydimethylsiloxane (PDMS) from DOW CORNING is spun onto the copper electrodes and cured at 80°C for 2 hours. The PDMS layer insulates the electrodes from the microfluidic channel that will later be attached to the IMS.

(g) *Substrate for SU-8 master:* A 3" silicon wafer (single-side polished) is used as the SU-8 mold substrate. Piranha cleaning (3:1 H_2SO_4: H_2O_2) and a dehydration bake of the substrate improves the eventual adhesion of SU-8.

(h) *SU-8 photoresist spin-on:* After the dehydration bake, SU-8 photoresist is spun onto the silicon substrate. The thickness of SU-8 determines the PDMS microfluidic channel height (100 μm in this case).

(i) *SU-8 photoresist patterning:* After a soft bake, SU-8 photoresist is exposed under an EVG 620 mask aligner, post-baked and developed to create the final SU-8 master for the microfluidic channel.

(j) *Casting the PDMS mold:* 10:1 ratio PDMS pre-polymer base and curing agent are mixed and degassed in a vacuum desiccator. Before the PDMS mixture is poured, the SU-8 master is silanized for five minutes with tetramethylchlorosilane (TMCS) from ALDRICH. Once poured onto the silanized master, the mixture is again degassed and cured at 80°C in an oven for 2 hours.

(k) *PDMS removal:* Once cured, the PDMS microfluidic device is easily peeled off from the silanized SU-8 master, and fluidic connection holes are punched in. The SU-8 master can be reused many times to create more PDMS devices.

(l) *Microfluidic device to IMS attachment:* Treating the PDMS surfaces on both the microfluidic component and the IMS with plasma (in an air plasma chamber from HARRICK SCIENTIFIC) for one minute renders them hydrophilic and incorporates oxygen onto the surface; once aligned and pressed together, the two device components attach strongly via oxygen bonds. Baking the composite structure at 65°C for about half an hour enhances the attachment further.

(m) *Final assembly:* Attaching tubing and pressure sensors to the microfluidic device completes the fabrication process.

The actual device shown in Fig. 3 contains EMG 700 series water-based ferrofluid from FERROTEC in its microfluidic channels. Next generation devices will feature thick electrodes embedded in soft magnetic materials for optimal magnetic flux transfer to the ferrofluid [11].

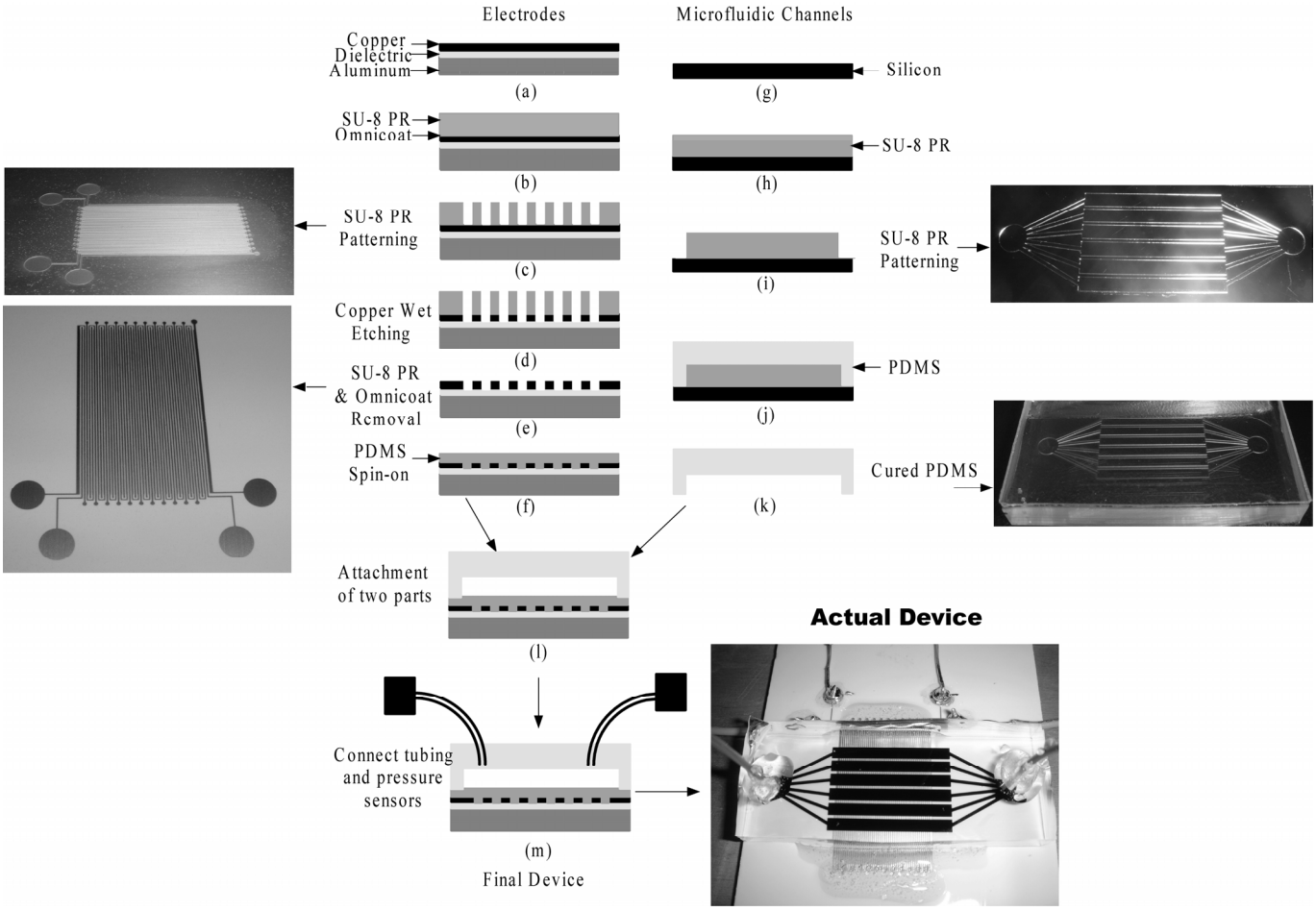

Fig. 3. Fabrication process steps for the ferrofluid micropump and pictures of the intermediate and completed device.

IV. EXPERIMENTAL RESULTS AND DISCUSSION

The first performance issue to be addressed is the ability of the substrate to accommodate relatively high current densities necessary for ferrofluid pumping. A significant temperature rise within the microchannel would adversely affect the pumping dynamics by reducing the overall magnetization of the ferrofluid. In that regard, the electrode substrate must allow good thermal contact between a heat sink and the copper electrodes. We tested the thermal performance of ferrofluid micropumps fabricated using glass epoxy and IMS based PC boards; the results are depicted in Fig. 4. It is clear that the temperature rise of the liquid within the microfluidic channel of the glass epoxy PC board is much larger than that of the IMS-based device. An external aluminum heat sink helps the glass epoxy PCB dissipate heat faster, but the insulated metal substrate is still a much better choice for this application.

The Brownian relaxation time constant (τ) of a ferrofluid is given by $4\pi r^3\eta_0/kT$, where r is the overall effective radius of the nanoparticles (a mode of 6.5 nm for EMG 700); η_0 is the viscosity of liquid (4.5 cp); k is the Boltzmann constant and T is the temperature (300 K). Based on the discussion in the theory section above, the ferrofluid pumping peak frequency is therefore expected to be around 42 kHz. Fig. 5 compares the experimental ferrofluid pumping characteristics of the micropump to the predictions of the theory [9]. Since static pumping pressure, and not fluid velocity, is measured, the numerical models are run iteratively to determine the pressure differential that results in stopped flow. The only fit parameter in the simulation is the magnitude scaling of the signal; the uncertainty arises from the difficulty of absolute pressure calibration of the sensors. Notice, however, that the pumping peak location is where it is expected. The experimental pumping curve depicted in Fig. 5 deviates in at least two ways from the simple theory that assumes a monodisperse suspension of particles and constant environmental conditions. First, at relatively very low frequencies, there is a minor pumping peak associated with a certain fraction of particles forming small agglomerates in the presence of the applied fields. The frequency of that minor pumping peak (around 1 kHz) indicates an effective hydrodynamic radius about three times that of the median. Secondly, there is a clear discrepancy between experiment and simple theory as the excitation frequency is increased beyond the main pumping peak. We believe this discrepancy is due to eddy-current heating of the aluminum layer of the IMS, and gets worse with increasing frequency. Increasing ferrofluid temperature lowers the Brownian relaxation time constant and reduces pumping at high frequencies. Next generation devices will

feature fully insulating, thermally high conductive PCB substrates to alleviate this phenomenon.

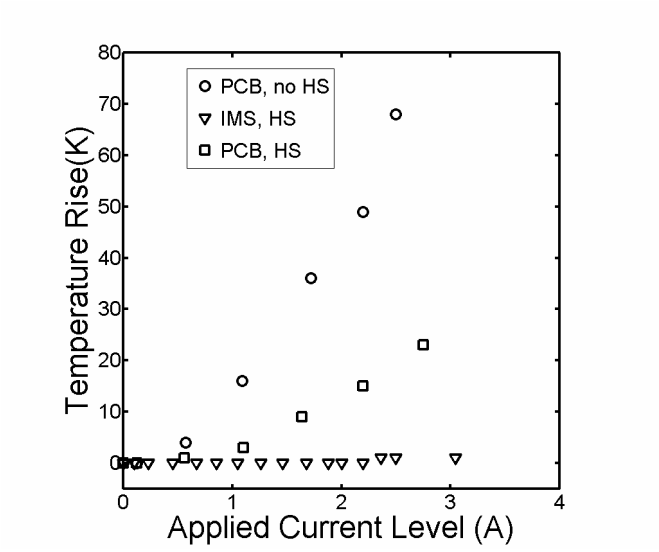

Fig. 4. Temperature rise versus applied current level (peak-to-peak amplitude) for two kinds of substrates. PCB represents the commonly used PC boards with copper layer on glass epoxy; IMS is the thermal clad insulated metal substrate. HS stands for heat sink, which in our experiment is a 6 inch by 6 inch, 2cm thick aluminum piece. Temperature rise is measured using a thermocouple close to the copper electrodes once an AC current (at 1 kHz) is applied for 6 minutes to reach steady state.

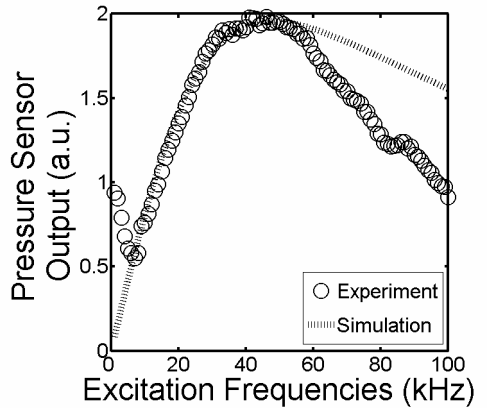

Fig. 5. Experimental results and a theoretical fit for the pumping characteristics of an EMG 700 series water-based ferrofluid in the micropump device.

V. CONCLUSIONS

We have reported the fabrication process and experimental results of a ferrofluid micropump. The thermal clad insulated metal substrate is used to fabricate the pumping electrodes to deliver effective heat dissipation. Our theory successfully predicts the peak location of ferrofluid pumping based on Brownian relaxation dynamics of the magnetic nanoparticles inside the carrier liquid. The next step in the device development will involve fabricating the micropump on a PCB with an electrically insulating, thermally conductive backboard. Once prototyping is completed, the eventual devices will be engineered on a silicon substrate with integrated electronics and a closed-loop microchannel geometry for cellular manipulation and other lab-on-a-chip applications.

VI. ACKNOWLEDGMENTS

The authors would like to thank Prof. Markus Zahn for insightful discussions. We are grateful to Prof. Eric Dufresne for viscosity measurements and to Dr. K. Raj of FERROTEC for the ferrofluid sample. This work was in part supported by the National Science Foundation (ECS-0449264).

VII. REFERENCES

[1] R. E. Rosensweig, "Ferrohydrodynamics," Cambridge University Press, Cambridge: 1985.

[2] K. Raj and R. Moskowitz, "Commercial applications of ferrofluids," *Journal of Magnetism and Magnetic Materials,* vol. 85, 1990, pp. 233-245.

[3] A. Hatch, A. E. Kamholz, G. Holman, P. Yager and K. F. Bohringer, "A ferrofluidic magnetic micropump," *Journal of Microelectromechanical systems*, vol. 10, no. 2, 2001, pp. 215-221.

[4] G. S. Park and S. H. Park, "Design of Magnetic Fluid Linear Pump," *IEEE Transactions on Magnetics*, vol. 35, no. 5, 1999, pp. 4058-4060.

[5] M. Shinkai, "Functional magnetic particles for medical applications," *Journal of Bioscience and Bioengineering,* vol. 94, no. 6, 2002, pp. 606-613.

[6] M. Zahn and D. R. Greer, "Ferrohydrodynamic pumping in spatially uniform sinusoidally time-varying magnetic fields," *Journal of Magnetism and Magnetic Materials*, vol. 149, no. 1-2, 1995, pp. 165-173.

[7] L. Mao and H. Koser, "Ferrohydrodynamic pumping in spatially traveling sinusoidally time-varying magnetic fields," *Journal of Magnetism and Magnetic Materials*, vol. 289, 2005, pp. 199-202.

[8] L. Mao and H. Koser, "Modeling ferrofluids in spatially-traveling sinusoidally time-varying magnetic fields," *3rd International Conference Computational modeling and simulation of materials*, Sicily, Italy, 2004, pp. 381-388.

[9] L. Mao and H. Koser, "An integrated, high flow rate MEMS ferrofluid pump," *9th International Conference on Miniaturized Systems for Chemistry and Life Sciences (μTAS)*, Boston, USA, 2005.

[10] Y. Xia and G. M. Whitesides, "Soft lithography," *Annual Review of Materials Science*, vol. 28, 1998, pp. 153-184.

[11] H. Koser, F. Cros, M. G. Allen, and J. H. Lang, "A High Torque Density Magnetic Induction Machine, " *11th Int. Conf. on Solid-State Sensors and Actuators (Transducers)*, Munich, Germany, 2001, pp. 284.